Sensitivity of the excitation functions of collective flow to relativistic scalar and vector meson interactions in the relativistic quantum molecular dynamics model RQMD.RMF

Yasushi Nara [1,2] and Horst Stoecker [2,3,4]

[1]*Akita International University, Yuwa, Akita city 010-1292, Japan*
[2]*Frankfurt Institute for Advanced Studies, D-60438 Frankfurt am Main, Germany*
[3]*Institut für Theoretishe Physik, Johann Wolfgang Goethe Universität, D-60438 Frankfurt am Main, Germany*
[4]*GSI Helmholtzzentrum für Schwerionenforschung GmbH, D-64291 Darmstadt, Germany*

Relativistic quantum molecular dynamics with scalar and vector interactions based on the relativistic mean meson field theory, RQMD.RMF, is developed. It is implemented into the microscopic transport code JAM, which includes both hadron resonances from the PDG book and string degrees of freedom. The sensitivity of the directed and of the elliptic proton flow in high energy heavy-ion collisions on the stiffness of the RMF equation of state (EoS) is examined. These new calculations are compared to high statistics experimental data at mid-central Au + Au collisions in the beam energy range $2.5 < \sqrt{s_{NN}} < 20$ GeV. This new RQMD model with the relativistic mean-field scalar and vector meson interactions does describe consistently, with one RMF parameter set, the beam energy dependence of both the directed flow and the elliptic flow, from SIS18 to AGS and RHIC BES-II energies, $\sqrt{s_{NN}} < 10$ GeV. This is interesting, as there are different sensitivities of these different kinds of flow to the EoS: elliptic flow is most sensitive to the nuclear incompressibility constant, at the moderate beam energies $\sqrt{s_{NN}} < 3$ GeV, whereas the directed flow is most sensitive to the effective baryon mass at saturation density at $3 < \sqrt{s_{NN}} < 5$ GeV. This self-consistent relativistic N-body hadronic transport approach describes well the experimental flow data up to higher beam energies, $\sqrt{s_{NN}} < 10$ GeV, by a stiff, monotonous EoS. Matters abruptly change in the next higher energy range, $\sqrt{s_{NN}} \gtrsim 10$–20 GeV: the directed flow data show a double change of sign of the slope of v_1, inverting twice in this energy range, in sudden contradiction to the RQMD.RMF calculation for a monotonous, stiff EoS. This surprising oscillating behavior, a double change of sign of the v_1 slope, points to the appearance of a hitherto unknown first-order phase transition in excited QCD matter at high baryon densities in mid-central Au + Au collisions.

I. INTRODUCTION

The phase structure of QCD in different regions of the T-μ_B phase diagram [1] is of fundamental interest in nuclear and astrophysics: the structure and the maximum mass of neutron stars and the dynamics of binary neutron star collisions, as observed in gravitational wave detectors, as well as the subsequent black hole formation and supernova explosions depend sensitively on the stiffness of the nuclear equation of state at high temperature and density [2]. Hence, substantial effort has been devoted by theorists and experimentalists alike to measure the equation of state (EoS) in the laboratory [3–10]. New phases of hot and dense nuclear matter can be formed in microscopic quantities in high energy heavy-ion collisions; there, experimental data can reveal the phase properties by unexpected changes of physical observables when varying the beam energy (the excitation function), the system size, and the centrality of the colliding systems.

This search for a conjectured first-order phase transition and the critical end point at high baryon density QCD matter is a challenging goal of high energy heavy-ion collision research [11]. Different species of collective flow are observed in high energy heavy-ion collisions, which result from a complex interplay between the initial state geometry, non-equilibrium effects and viscosity, and the equation of state—the pressure, which acts as a barometer for the bulk properties of strongly interacting compressed and highly excited nuclear matter. Anisotropic flows, such as the directed flow $v_1 = \langle \cos \phi \rangle = \langle p_x/p_T \rangle$ and the elliptic flow $v_2 = \langle \cos 2\phi \rangle = \langle (p_x^2 - p_y^2)/p_T^2 \rangle$, are generated by the pressure already during the early stages of the collisions. Here ϕ is the azimuthal angle with respect to the reaction plane. Distinct flow coefficients serve as sensitive messengers (barometers) of the EoS [3–10]. Large elliptic flow had been observed experimentally both at the fixed target accelerators Bevalac, SIS, AGS, and SPS, as well as at the colliders RHIC and LHC. The measured flow is in reasonably good agreement with hydrodynamic simulations [12–18].

The ongoing Beam Energy Scan (BES) program [19,20] at the BNL-RHIC-STAR and the CERN-SPS-NA49 and -NA61/SHINE experiments [21] seek to find the conjectured "point of onset of deconfinement" (CPOD) and the conjectured associated critical point (CP). Future experiments, such as RHIC-BES-II [22], STAR-FXT, CBM and HADES at FAIR [23,24], BM@N and MPD at NICA [25], HIAF at Canton, as well as the proposed J-PARC-HI [26] will offer

excellent high statistics data which will allow to explore the highest density baryonic matter sector of QCD, and reveal the phase structure of QCD at high baryochemical potential $\mu_B \approx 1$ GeV.

Significant progress in modeling heavy-ion collisions at high baryon density is in order to interpret the wealth of the new data. Improved ideal and viscous hydrodynamic theory and transport models have been developed over the last decade, simulating the dynamics of high energy heavy-ion collisions [27–31]. To date, all these models have not been successful in explaining and reproducing the unique prediction of the strange looking "double change of sign," from a positive slope of v_1 to a negative slope and back to a positive slope of v_1, for mid-rapidity protons in Pb + Pb collisions, which should only occur if there is a first-order phase transition in the dense baryonic matter (see Ref. [10] and references therein).

These predicted negative proton v_1 slopes were observed with moderate statistics more than a decade ago at $\sqrt{s_{NN}} =$ 8.8 and 17.3 GeV by the NA49 Collaboration in fixed target experiments at the SPS [32]. The heavy-ion beam energy dependence of the directed flow of all hadrons, baryons, and mesons was measured recently with much higher statistics and in smaller steps in the BES, from $\sqrt{s_{NN}} = 7.7$ to 200 GeV, by the STAR Collaboration at BNL's RHIC facility. Here, the predicted drastic double change of sign of the directed flow was now clearly discovered, with negative mid-rapidity slopes for both the net proton and the net lambda directed flow between $\sqrt{s_{NN}} = 11.5$ and 19.5 GeV [33,34], in near central Au-Au collisions. This signal can easily be distinguished from the monotonous negative proton v_1 flow predicted for peripheral collisions at high energy $\sqrt{s_{NN}} > 30$ GeV: There, secondary interactions, which only start after the two nuclei have passed through each other, cause this geometrical effect, which does not predict a double change in sign as a function of energy [35]. All standard microscopic transport models which do not implement a first-order phase transition fail to reproduce the negative proton v_1 slope with double change of sign at around $\sqrt{s_{NN}} = 8.8$–19.6 GeV [36,37]. In "ideal fluid" relativistic hydrodynamics, i.e., without a first-order phase transition, there is also no change in sign of v_1 predicted. However, if a first-order phase transition is put into the fluid's EoS, it generates negative v_1 values at the heavy-ion energy around the "softest point," $\sqrt{s_{NN}} \approx 3$–5 GeV. This seems to be in contradiction to the positive v_1 data observed at the AGS [38,39]. Three-fluid model (3FD) simulations [40] predict a minimum in the excitation function for the slope of v_1 at $\sqrt{s_{NN}} \approx 6$ GeV. Hadronic transport model calculations with strongly attractive mean fields, supposedly simulating the effect of a first-order phase transition, show antiflow at AGS energies [41]. Microscopic transport models which take into account the effects of the softening by the modified collision term also predict the negative flow at $\sqrt{s_{NN}} = 3$–5 GeV [42,43]. Hybrid models such as hydro + UrQMD [44] show no sensitivity of the directed flow on details of the EoS.

Microscopic transport models have been extensively employed to study the dynamics of nuclear collisions (see Ref. [45] for the recent comparison of heavy-ion transport codes). Microscopic transport models such as single-particle density Boltzmann-Uehling-Uhlenbeck (BUU) [46,47] and Vlasov-Uehling-Uhlenbeck (VUU) [48] and N-body quantum molecular dynamics (QMD) models [49] have been widely used to simulate the space-time dynamics of nuclear collisions. These approaches used non-relativistic Skyrme forces, where the single-particle potentials are given by baryon density (ρ_B) dependent attractive and repulsive terms and momentum dependent terms [50–52]:

$$V_{sk} = \alpha \rho_B + \beta \rho_B^\gamma + C \int d^3 p' \frac{f(x, p')}{1 + (\boldsymbol{p} - \boldsymbol{p}')^2/\Lambda^2}. \quad (1)$$

However, these non-relativistic approaches do not reproduce the observed beam energy dependencies of either the directed or the elliptic flow, if a single Skyrme parameter set is used [9,53–57]; it seems that a hard EoS is required at lower beam energies $\sqrt{s_{NN}} < 3$ GeV, and a soft EoS is favored at higher beam energies. It was suggested that this provides evidence for a softening of the EoS, and even for the onset of the conjectured first-order phase transition.

A relativistic transport approach, based on the single-particle density relativistic meson mean-field theory (RMF) has been developed, called RBUU [52,58], RVUU [59], or RLV [60]. In these covariant approaches, relativistic meson mean fields are implemented instead of non-relativistic Skyrme potentials. These meson fields interact with the baryons via scalar and vector meson couplings. This is very different from the non-relativistic potential approaches. It was demonstrated that the beam energy dependence of both the sidewards $\langle p_x \rangle$ and the elliptic flow are reproduced, up to top AGS energies $\sqrt{s_{NN}} < 5$ GeV, within this RBUU model, only if the scalar and vector form factors at the vertices cut off the interaction at high momenta ($p > 1$ GeV/c) [61]. A similar relativistic mean-field approach was also implemented into the framework of the relativistic N-body quantum molecular dynamics (RQMD) approach (see Ref. [62]) and used for simulating heavy-ion collisions up to $E_{\text{lab}} \leqslant 2A$ GeV; here only a few hadron resonances were included, but the effects of the density dependence of the coupling constants of the meson mean fields on the transverse flow were studied.

The N-body RQMD approach with relativistic meson mean fields and a large number of PDG hadrons and resonances had not been developed to date. That input is clearly most important for describing heavy-ion experiments at higher energy: at the AGS and SPS, numerous high mass hadrons and resonances with additional conserved charges, like strangeness and charm, are produced in the collisions, and multi-particle production, efficiently described by string and Hagedorn bag models, plays an important role.

This paper presents the implementation of the relativistic meson mean fields into the relativistic Hamiltonian N-body RQMD code JAM with a wealth of PDG book baryons, mesons, and hadronic resonances as well as strings included. This allows to investigate the N-body multi-hadron collision dynamics, beyond the time evolution of single-particle distribution functions like the RBUU approach. In this paper, we specifically examine the beam energy dependence of the directed and elliptic flow in the beam energy range $\sqrt{s_{NN}} = 2.5$–20 GeV within the RQMD.RMF approach, where the

scalar and vector interactions are implemented in the microscopic transport code JAM [63].

This paper is organized as follows: Section II describes the non-linear σ-ω model and its implementation into the RQMD framework. Section III presents the results for the beam energy dependence of the directed and the elliptic flows, as well as the rapidity dependence of the directed flow. The high sensitivity of the directed flow at forward-backward rapidity on the relativistic mean-field interactions is emphasized. The summary is given in Sec. IV.

II. MODEL

Here, relativistic mean-field interactions of the most abundant PDG hadrons are implemented for the first time into the relativistic N-body propagation protocol of RQMD, as realized in the transport code JAM [63]. The code is prepared to simulate nuclear collisions up to $\sqrt{s_{NN}} \approx 30$ GeV. The collision term of RQMD-JAM models particle production by the excitations of hadrons, hadronic resonances, and strings and their decays, analogously as in the original RQMD code[1] and UrQMD models [66,67]. Secondary products are allowed to re-scatter, which generates collective effects within the RQMD.RMF approach. Details of the collision term in JAM can be found in Ref. [63].

A. Relativistic mean field

The relativistic mean-field theory employed here uses σ and ω meson-baryon interactions. The corresponding equilibrium thermodynamics yields the energy density for nuclear matter:

$$e = \int d^3 p E^* f(p) + \frac{1}{2} m_\omega^2 \omega^2 + U(\sigma). \quad (2)$$

Here $f(p)$ is the Fermi-Dirac distribution for the different baryon species. The second term contains the ω contribution as the zeroth component of the vector potential ω^μ. The spatial components vanish in uniform, stationary nuclear matter. The single-particle energy $E^* = \sqrt{m^{*2} + p^2}$ contains the single-particle scalar potential S,

$$m^* = m - S = m - g_s \sigma, \quad (3)$$

through the linear coupling of the σ meson field to the baryon. This modifies the value of the vacuum nucleon mass $m = 938$ MeV in the medium. We consider here also Boguta's non-linear self-interactions of the scalar field [68],

$$U(\sigma) = \frac{m_\sigma^2}{2} \sigma^2 + \frac{g_2}{3} \sigma^3 + \frac{g_3}{4} \sigma^4. \quad (4)$$

---

[1]Here the term RQMD is used as the name of the code developed by Sorge, Stoecker, and Greiner [64,65]. However, the term RQMD is here also used for the underlying theoretical N-body model, i.e., the relativistic extension of the N-body QMD model. Several groups have developed RQMD codes by using approximations to and based on the RQMD formalism by Sorge, Stoecker, and Greiner. We use the term RQMD for the theoretical approach throughout this paper.

TABLE I. Parameters for the relativistic mean-field theory with non-linear scalar interaction for a binding energy of $B = -16$ MeV and for normal nuclear matter density of $\rho_0 = 0.168$ 1/fm^3. A σ mass of $m_\sigma = 2.79$ 1/fm and an ω mass of $m_\omega = 3.97$ 1/fm are used.

Type	K (MeV)	m^*/m	g_s	g_v	g_2 (1/fm)	g_3
NS1	230	0.800	8.182	7.721	31.623	−3.7977
NS2	380	0.800	7.211	7.721	−17.889	197.64
NS3	380	0.722	8.562	9.601	0.4429	44.704

The σ field is obtained by solving the self-consistent equation

$$m_\sigma^2 \sigma + g_2 \sigma^2 + g_3 \sigma^3 = g_s \rho_s. \quad (5)$$

Here $\rho_s = \int d^3 p \frac{m^*}{E^*} f(p)$ is the scalar baryon density. The coupling constants which reproduce nuclear matter saturation values for a given incompressibility constant K and for a given effective nucleon mass m^* at ground state nuclear density are given in Table I.

Figure 1 compares the energy per nucleon at zero temperature as a function of the baryon density for different parameter sets. Note that parameter sets with equal effective masses yield similar EoS (see, e.g., NS1 and NS2). Also note that smaller effective masses always yield stiffer EoS, i.e., hard repulsion at high densities, even if the ground state incompressibility constant is not large. For instance, NS2 ($m^*/m = 0.8$) and NS3 ($m^*/m = 0.722$) have identical ground state $K = 380$ MeV values, but at high density, NS2 is much softer than NS3. This behavior is due to the fact that the effective mass at saturation density determines the strength of the vector interaction $C_v = g_v/m_\omega$, which is independent of the scalar interaction term due to the Weisskopf relation:

$$\sqrt{m^{*2} + p_F^2(\rho_0)} + C_v \rho_0 = m + B. \quad (6)$$

Here $p_F = (3/2\pi^2 \rho_0)^{2/3}$ is the Fermi momentum at saturation density, and $B = -16$ MeV is the ground state binding energy per particle of infinite nuclear matter. Hence, the hardness of the EoS is nearly linearly related to the effective baryon
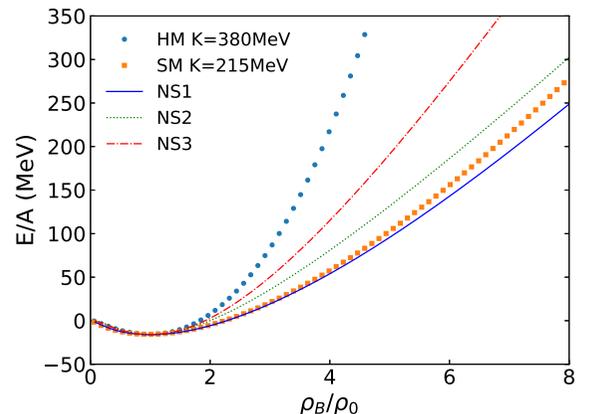

FIG. 1. Total energy per nucleon as a function of the normalized baryon density at zero temperature.

mass at high baryon densities. The hardness is barely sensitive to the ground state incompressibility as was pointed out in Refs. [69,70]. For comparison, the E/A values for the non-relativistic Skyrme potential [Eq. (1)], for a hard EoS with $K = 380$ (circles) and a soft EoS with $K = 215$ MeV (squares) [52], are plotted as a function of the baryon vector density. Note that the non-relativistic Skyrme potential yields a similar E/A as a function of the vector density as the soft relativistic parameter set with $m^*/m = 0.8$ (NS1 and NS2).

B. Relativistic quantum molecular dynamics

The different relativistic EoS are now implemented into the framework of the RQMD approach [64], formulated based on the constraint Hamiltonian dynamics [71] to simulate the N-body non-equilibrium dynamics.

$8N$ four-vectors q_i^μ and p_i^μ $(i = 1, \ldots, N)$ are used throughout the manifestly covariant formalism for the N-body dynamics. In order to reduce the number of dimensions from $8N$ to the physical $6N$, $2N$ constraints are employed, namely,

$$\phi_i \approx 0 \quad (i = 1, \ldots, 2N), \tag{7}$$

where the sign $\approx$ stands for Dirac's weak equality: this equality has to be satisfied on the physical $6N$ phase space. $2N - 1$ Poincaré invariant constraints are used, while the $2N$th constraint determines the evolution parameter τ, which is not necessarily Poincaré invariant. The Hamiltonian of the system is constructed as the linear combination of $2N - 1$ constraints

$$H = \sum_{j=1}^{2N-1} u_j(\tau)\phi_j \tag{8}$$

with the Lagrange multipliers $u_j(\tau)$. The equations of motion are given by

$$\frac{dq_i}{d\tau} = [H, q_i] \approx \sum_{j=1}^{2N-1} u_j \frac{\partial \phi_j}{\partial p_j},$$

$$\frac{dp_i}{d\tau} = [H, p_i] \approx -\sum_{j=1}^{2N-1} u_j \frac{\partial \phi_j}{\partial q_j}, \tag{9}$$

where the Poisson brackets are defined as

$$[A, B] = \sum_k \left(\frac{\partial A}{\partial p_k} \cdot \frac{\partial A}{\partial q_k} - \frac{\partial B}{\partial q_k} \cdot \frac{\partial B}{\partial p_k} \right). \tag{10}$$

The constraints are conserved in time:

$$\frac{d\phi_i}{d\tau} = \frac{\partial \phi_i}{\partial \tau} + [H, \phi_i] \approx 0. \tag{11}$$

As $2N - 1$ constraints do not depend explicitly on τ, the Lagrange multipliers u_i are solved as

$$u_i \approx -\frac{\partial \phi_{2N}}{\partial \tau} C_{2N,i} \quad (i = 1, \ldots, 2N - 1), \tag{12}$$

where $C_{ij}^{-1} = [\phi_i, \phi_j]$. Thus, the trajectory of the coupled system of particles in $6N$ phase space is uniquely determined by the equations of motion [Eqs. (9)] together with the Lagrange multipliers [Eq. (12)].

Here, N on-mass shell conditions are imposed:

$$\phi_i \equiv p_i^{*2} - m_i^{*2} = (p_i - V_i)^2 - (m_i - S_i)^2 \quad (i = 1, \ldots, N) \tag{13}$$

for the ith particle, where V_i^μ and S_i are the single-particle vector and scalar potentials, which are functions of the baryon current J_i^μ and scalar density ρ_{si}. Within the RQMD approach, these densities of the ith particle are influenced by all the other particles,

$$\rho_{s,i} = \sum_{j \neq i} \frac{m_j^*}{p_j^{*0}} \rho_{ij}, \quad J_i^\mu = \sum_{j \neq i} B_j v_j^{*\mu} \rho_{ij}, \tag{14}$$

here $v_j^{*\mu} = p_j^{*\mu}/p_j^{*0}$ and B_j are, respectively, the velocity and the baryon number of the jth particle, while ρ_{ij} is the so-called interaction density (the overlap of density with other hadron wave packets) given by the Gaussian in RQMD:

$$\rho_{ij} = \frac{\gamma_{ij}}{(4\pi L)^{3/2}} \exp\left(q_{Tij}^2/4L\right). \tag{15}$$

q_{Tij} is the center-of-mass frame distance between the particles i and j, and γ_{ij} is the respective Lorentz γ-factor which ensures the correct normalization of the Gaussians [72]. Throughout this work, the Gaussian width is fixed at $L = 1.0$ fm^2.

In addition to the N on-mass shell constraints of Eq. (13), the time fixation constraints, which equate all time coordinates of particles in the computational frame, follow the Maruyama model [73] and Ref. [74] for the rest of the N constraints:

$$\phi_{i+N} \equiv \hat{a} \cdot (q_i - q_N) \quad (i = 1, \ldots, N - 1),$$

$$\phi_{2N} \equiv \hat{a} \cdot q_N - \tau, \tag{16}$$

where $\hat{a}$ is a four-dimensional vector and is a unit vector $\hat{a} = (1, \mathbf{0})$ in the reference frame [73]. Hence, $\hat{a}$ must be changed under Lorentz transformation into other frames to maintain the Lorentz covariance. A convenient choice is $\hat{a} = P/\sqrt{P^2}$ with $P = \sum_i^N p_i$. Then the clock time of all particles is the same in the total center-of-mass system; it becomes the unit vector $(1, \mathbf{0})$ in the center-of-mass frame [74]. By choosing those $2N$ constraints, together with the assumption that the arguments of the potentials are replaced by the free ones, the equations of motion are obtained for particle i:

$$\dot{\mathbf{x}}_i = \frac{\mathbf{p}_i^*}{p_i^{*0}} + \sum_j^N \left(\frac{m_j^*}{p_j^{*0}} \frac{\partial m_j^*}{\partial \mathbf{p}_i} + v_j^{*\mu} \frac{\partial V_{j\mu}}{\partial \mathbf{p}_i} \right),$$

$$\dot{\mathbf{p}}_i = -\sum_j^N \left(\frac{m_j^*}{p_j^{*0}} \frac{\partial m_j^*}{\partial \mathbf{r}_i} + v_j^{*\mu} \frac{\partial V_{j\mu}}{\partial \mathbf{r}_i} \right). \tag{17}$$

Note that the equations of motion for non-relativistic QMD are recovered easily by neglecting the scalar potential and taking only the time component of the vector potential into account.

The actual simulations evaluate the non-linear σ field as well as the ω field at each space-time point using a local density approximation [52,58,59]; neglecting the derivatives of the meson fields as in Eq. (5) for the σ field, the vector

potential is simply proportional to the baryon current. This approximation is widely applied to high energy nuclear collision simulations [75–77]. There, the meson field radiation and retardation effects [78] were found to be on the percent level. The present study uses identical coupling constants for all baryons.

Note that the above mean-field interactions are combined with the collision term, which applies Monte Carlo methods to evaluate the scattering kernel. These collision terms treat the change of the potentials due to scattering as small at high energies as compared to the momenta of the outgoing particles. Hence, the treatment of the final state phase space factors for the outgoing particles is the same as in cascade simulations. Changes of the effective masses are taken into account for outgoing particles of different species. The violation of the global and local energy conservation is found to be less than 1%. A detailed discussion of the collision term treatment is found in Ref. [79]. Relativistic on- and off-shell parton scattering was recently studied [80] by basing the scattering processes on explicit matrix elements squared, which are well defined also off-shell, hence incorporating the changes of the final-state phase space by default.

III. RESULTS

A. Beam energy dependence of the flow

The upper panel of Fig. 2 compares the beam energy dependence of the slope of the proton directed flow at mid-rapidity ($|y| < 0.8$) from the JAM calculations in the RQMD.RMF mode (JAM/RQMD) with the E895 [81], NA49 [32,82], and STAR [33,34,83] experimental data. Only for the parameter sets NS1 ($K = 230$ MeV) and NS2 ($K = 380$ MeV) is good agreement with the data found, up to $\sqrt{s_{NN}} = 7.7$ GeV, nicely demonstrating the insensitivity of the directed flow to the incompressibility constant at the ground state density ρ_0. The fact that the NS3 parameter set simulations significantly overestimate the v_1 data clearly demonstrates the strong dependence of the directed flow on the baryons' effective mass. The directed flow is—up to maximum AGS/SIS100 energies—not sensitive to the incompressibility constant at the ground state density, but shows a strong sensitivity to the effective mass at saturation density. A strong influence of the effective mass on the directed flow at the lower BEVALAC/SIS18 energies ($E_{lab} = 1$–$2A$ GeV) had been found in both RBUU and RVUU calculations [58,59]. The reason for this strong dependence on m^* is that smaller effective masses imply larger values of the ω meson coupling constant, hence the stronger repulsion. An earlier approach based on non-relativistic Skyrme potentials with $K = 210$ MeV [9] seems to correspond to the parameter sets NS1 and NS2; both give the same hardness of the EoS.

The model predicts at beam energies $\sqrt{s_{NN}} > 8$ GeV still positive v_1 slopes; the directed flow slope at mid-rapidity here was insensitive to the EoS. Because the model yields nearly the same results as the cascade model, it indicates that mean-field effects are very weak on v_1 at mid-rapidity at SPS energies. The experimental data, however, show negative v_1 slopes at $\sqrt{s_{NN}} = 10$–20 GeV. It has been argued that this is

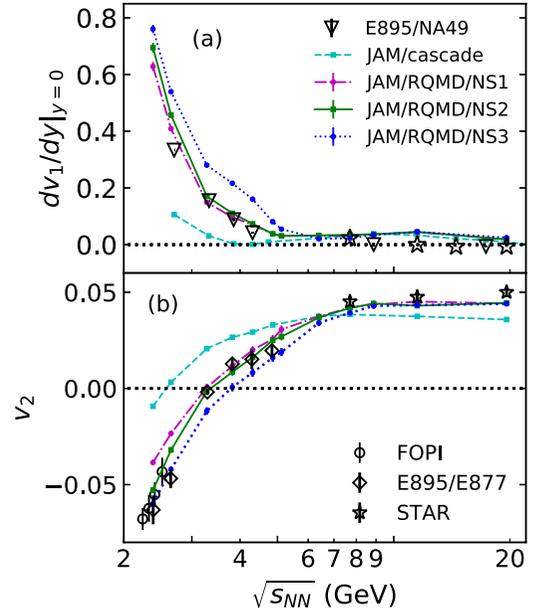FIG. 2. Beam energy dependence of (a) proton v_1 slope and (b) v_2 ($|y| < 0.2$) at mid-rapidity in mid-central Au+Au collisions ($4.6 \leqslant b \leqslant 9.4$ fm) from the JAM cascade (dashed lines), RQMD/NS1 (dash-dotted lines), RQMD/NS2 (solid lines), and RQMD/NS3 (dotted lines). The slopes of the proton v_1 are obtained by fitting the rapidity dependence of v_1 to a cubic equation at $|y| < 0.8$. The experimental v_1 data are taken from the E895 [81], NA49 [32,82], and STAR [33,34,83] Collaborations, respectively. The STAR data [84] for v_2 are for charged hadrons, while the data points by E895/E877 [53] and by FOPI [85] are for protons. The JAM v_2 values are for protons at $\sqrt{s_{NN}} < 5$ GeV, while the higher energy data are for charged particles.

an indication of the softening of the EoS. However, note that theoretical calculations which implement a first-order phase transition do predict negative v_1 slopes for protons at AGS energies, $\sqrt{s_{NN}} < 5$ GeV, but not at SPS energies [38,39,41–43]. The present results, which are for an EoS without a high density phase transition, do not reproduce the observed negative v_1 data at $\sqrt{s_{NN}} > 8$ GeV. Is this the long-sought-after first-order QCD-deconfinement phase transition?

The lower panel of Fig. 2 compares the beam energy dependence of the elliptic flow v_2 of the present RQMD.RMF model with experimental heavy-ion data of the FOPI [85], E897/E877 [53], and the STAR [84] Collaborations. At lower beam energies ($\sqrt{s_{NN}} < 10$ GeV), the strength of the elliptic flow is the result of the interplay between out-of-plane (squeeze-out) and in-plane emission [6,86]. Pure cascade models lack the pressure to generate the observed strong out-of-plane emission (negative v_2) at low beam energies and result in the larger (positive sign) elliptic flow at $\sqrt{s_{NN}} < 5$ GeV. A previous work predicted a strong enhancement of v_2 [87,88], as well as of v_4 [89], when a first-order phase transition occurs. This is due to the suppression of the squeeze-out as a result of the softening of the EoS [90]. Here, just on the contrary, the strongly repulsive interactions suppress v_2.

Figure 2 demonstrates that elliptic flow is not sensitive to the ground state incompressibility constant anymore when
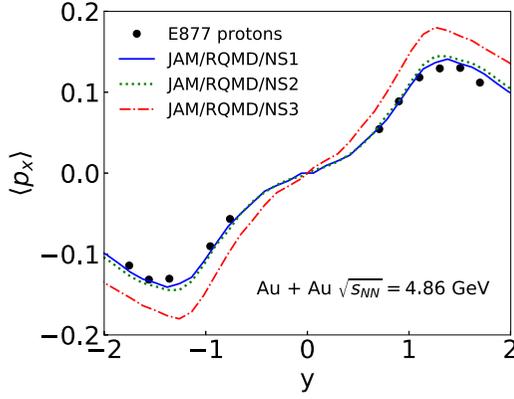
FIG. 3. Rapidity dependence of proton sideward flow $\langle p_x \rangle$ in mid-central Au + Au collision at $\sqrt{s_{NN}} = 4.86$ GeV from RQMD/NS1 (solid line), RQMD/NS2 (dotted line), and RQMD/NS3 (dot-dashed line) compared with the E877 experimental data [92].

$\sqrt{s_{NN}} \approx 5$ GeV; both the NS1 and the NS2 parameter sets yield very similar values of v_2 for beam energies $\sqrt{s_{NN}} > 5$ GeV. However, the calculations with NS1 show less squeeze-out at lower beam energies $\sqrt{s_{NN}} < 3$ GeV, while the NS2 parameter set yields reasonable agreement with the data. Thus at lower energies, elliptic flow is sensitive to the ground state incompressibility of the EoS.

The calculations with the relativistic mean field predict considerably larger v_2 values than the cascade calculations at SPS/BES-II energies. This agreement with the v_2 data at the SPS is remarkable, as the elliptic flow achieved with the Skyrme forces does not show an enhancement of v_2; the same small values as in the cascade calculations are found with Skyrme forces at the beam energies $\sqrt{s_{NN}} > 6$ GeV [88,91].

B. Rapidity dependence of the directed flow

The rapidity dependence of the directed flow shown in Fig. 3 compares the sidewards flow $\langle p_x \rangle$ in mid-central Au + Au collisions at $\sqrt{s_{NN}} = 4.89$ GeV, as computed from RQMD.RMF simulations with different parameter sets, to the E877 data [92]. The calculations using the NS3 parameter set ($m^*/m = 0.722$) yield stronger directed flow than those using the set NS2, even though the ground state incompressibility constants of both parameter sets NS2 and NS3 have the same value, $K = 380$ MeV. However, the directed flow results from using the NS1 ($K = 230$ MeV) parameter set are almost identical to the NS2 results, as it has the same effective mass parameter as NS1. Hence, the slope of the directed flow at mid-rapidity as well as its rapidity dependence is quite sensitive to the stiffness of the high density EoS, i.e., the effective mass parameter, but is practically insensitive to the ground state incompressibility constant at AGS/SIS100 energies.

Figure 4 shows the rapidity dependence of v_1 of protons (upper panel) and pions (lower panel) from JAM/cascade, JAM RQMD/NS1, and JAM attractive orbit mode in mid-central Pb + Pb collisions at 8.87 GeV together with the NA49 data [32]. NA49 observed the collapse of flow at mid-rapidity that is in good agreement with the JAM attractive orbit mode [42].
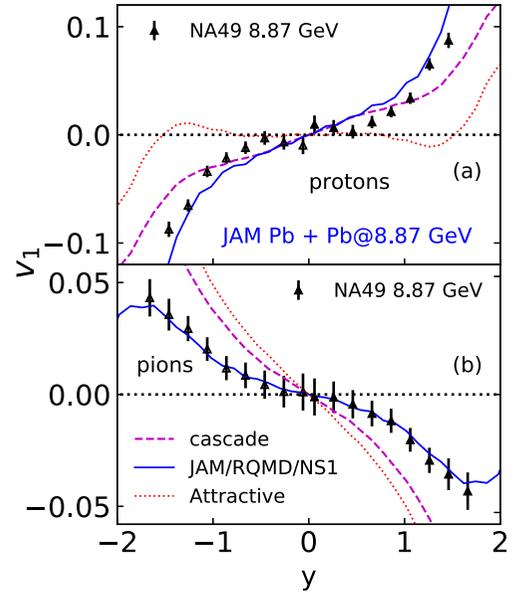

FIG. 4. Rapidity dependence of proton and pion v_1 in mid-central Pb+Pb collision at $\sqrt{s_{NN}} = 8.87$ GeV as calculated by the JAM cascade mode (dashed line), by RQMD/NS1 (solid line), and by JAM in the attractive scattering mode (dotted line). The calculations are compared to the NA49 Collaboration's experimental data [32].

The JAM attractive orbit mode selects only inwards scatterings ("attractive orbit mode") for all binary scatterings, to mimic the softening of the EoS. In stark contrast, calculations without a softening of the EoS, such as JAM/cascade and RQMD/NS1, clearly show no collapse of the directed flow
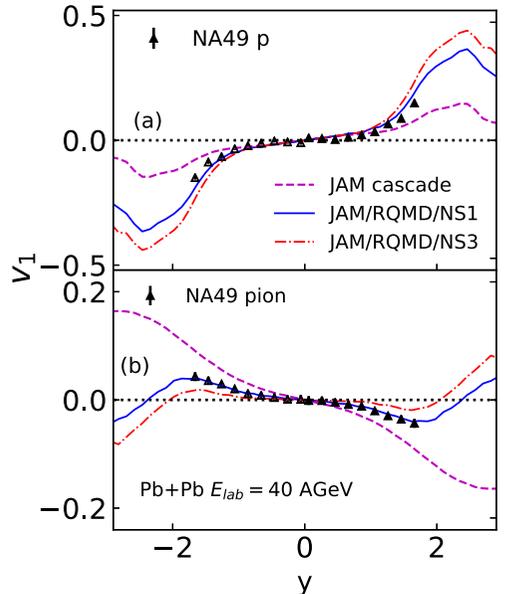

FIG. 5. Rapidity dependence of proton and pion v_1 in mid-central Pb+Pb collision at $\sqrt{s_{NN}} = 8.87$ GeV from the JAM cascade (dashed line), RQMD/NS1 (solid line), and RQMD/NS3 (dot-dashed line) are compared with the NA49 experimental data [32].

at all. Note that the RQMD/NS1 calculations show the same slope as the cascade results at mid-rapidity ($|y| < 0.5$). This may be because baryons are not fully stopped at this energy, and the baryon density at mid-rapidity is small, leading to a diminished strength of the baryon potential. In the present calculations, potential interactions of preformed hadrons are not included. They dominate the early stages of the collisions at 8.87 GeV. This is another reason that here is no effect of the potential on the mid-rapidity directed flow, which is most sensitive to the early compression stages of the collisions.

Figure 5 compares the calculated rapidity dependence of v_1 of protons and pions with the NA49 data [32] for a wider rapidity region. v_1 at forward rapidity, where the baryon density is large, does strongly depend on the EoS; it is very sensitive to the effective mass parameter, but insensitive to the incompressibility constant. At even higher beam energies, v_1 in forward-rapidity regions is still sensitive to the mean field. Hence, the v_1 data at forward rapidity contain valuable information about the EoS at high baryon density in high energy heavy-ion collisions.

IV. SUMMARY

Relativistic scalar and vector meson mean-field interactions are implemented into the JAM transport code based on the framework of the relativistic quantum molecular dynamics model (RQMD.RMF). The influence of the EoS on the beam energy dependence of anisotropic flow, both directed and elliptic flow, from SIS18 to AGS/SIS100 energies is reproduced by the same parameter set of the scalar-vector-type interaction. The elliptic flow at low energies $\sqrt{s_{NN}} < 3$ GeV is sensitive to the ground state incompressibility and the directed flow is sensitive to the ground state effective mass parameter in the EoS at energies $\sqrt{s_{NN}} < 5$ GeV. The experimentally observed negative proton directed flow at $10 < \sqrt{s_{NN}} < 20$ GeV cannot be explained by "normal," monotonously increasing relativistic mean fields, whereas the elliptic flow is in good agreement with the data for the whole energy region $2.5 < \sqrt{s_{MN}} < 20$ GeV. No EoS dependent change of sign of the directed flow is predicted in RQMD.RMF with the "normal" EoS, either for directed or for elliptic flow, at beam energies above $\sqrt{s_{NN}} > 10$ GeV at mid-rapidity. This does not imply that mean-field effects are negligible, as mean fields enhance strongly the elliptic flow at SPS energies relative to the cascade model. The directed flow at the forward-backward rapidity region depends strongly on the EoS.

References [93–95] studied the influence of the mean-field potentials on the cumulant ratios of protons within QMD models with Skyrme forces. Relativistic ω fields may suppress the kurtosis of the baryon number distribution at high baryon densities in mean-field nuclear matter calculations [96]. An investigation of such a suppression within the RQMD.RMF dynamical approach is under way.

The late hadronic fluid stage of collisions at RHIC/LHC energies is usually described by hadronic cascade models. However, the mean-field effects presented here may also be relevant for this late evolution stage of the hadronic fluid stage at RHIC/LHC energies. Observables such as baryon spectra at forward rapidity as well as flow v_1 and also v_2 can allow for a study of the mean-field effects on the final hadronic fluid stage on an event-by-event basis.

[1] Edited by B. Friman, C. Höhne, J. Knoll, S. Leupold, J. Randrup, R. Rapp, and P. Senger, in *The CBM Physics Book*, Lecture Notes in Physics, Vol. 814 (Springer, Berlin, Heidelberg, 2011), p. 1.

[2] E. R. Most, L. J. Papenfort, V. Dexheimer, M. Hanauske, S. Schramm, H. Stöcker, and L. Rezzolla, Phys. Rev. Lett. **122**, 061101 (2019).

[3] H. Stöcker, J. A. Maruhn, and W. Greiner, Phys. Rev. Lett. **44**, 725 (1980).

[4] H. Stöcker, L. P. Csernai, G. Graebner, G. Buchwald, H. Kruse, R. Y. Cusson, J. A. Maruhn, and W. Greiner, Phys. Rev. C **25**, 1873 (1982).

[5] G. Buchwald, G. Graebner, J. Theis, J. Maruhn, W. Greiner, H. Stöcker, K. Frankel, and M. Gyulassy, Phys. Rev. C **28**, 2349 (1983).

[6] H. Stoecker and W. Greiner, Phys. Rep. **137**, 277 (1986).

[7] C. Hartnack, J. Aichelin, H. Stoecker, and W. Greiner, Phys. Lett. B **336**, 131 (1994).

[8] J.-Y. Ollitrault, Phys. Rev. D **46**, 229 (1992).

[9] P. Danielewicz, R. Lacey, and W. G. Lynch, Science **298**, 1592 (2002).

[10] H. Stoecker, Nucl. Phys. A **750**, 121 (2005).

[11] M. Asakawa and K. Yazaki, Nucl. Phys. A **504**, 668 (1989); D. H. Rischke, Prog. Part. Nucl. Phys. **52**, 197 (2004); M. A. Stephanov, Prog. Theor. Phys. Suppl. **153**, 139 (2004); Int. J. Mod. Phys. A **20**, 4387 (2005); K. Fukushima and C. Sasaki, Prog. Part. Nucl. Phys. **72**, 99 (2013).

[12] U. Heinz and R. Snellings, Annu. Rev. Nucl. Part. Sci. **63**, 123 (2013).

[13] C. Gale, S. Jeon, and B. Schenke, Int. J. Mod. Phys. A **28**, 1340011 (2013).

[14] P. Huovinen, Int. J. Mod. Phys. E **22**, 1330029 (2013).

[15] T. Hirano, P. Huovinen, K. Murase, and Y. Nara, Prog. Part. Nucl. Phys. **70**, 108 (2013).

[16] S. Jeon and U. Heinz, Int. J. Mod. Phys. E **24**, 1530010 (2015).

[17] A. Jaiswal and V. Roy, Adv. High Energy Phys. **2016**, 9623034 (2016).

[18] P. Romatschke and U. Romatschke, *Relativistic Fluid Dynamics In and Out of Equilibrium*, Cambridge Monographs on Mathematical Physics (Cambridge University Press, Cambridge, 2019).

[19] S. Singha, P. Shanmuganathan, and D. Keane, Adv. High Energy Phys. **2016**, 2836989 (2016).

[20] J. Adam *et al.* (STAR Collaboration), Phys. Rev. C **99**, 064905 (2019).

[21] L. Turko (NA61/SHINE Collaboration), Universe **4**, 52 (2018); K. Grebieszkow (NA61/SHINE Collaboration), PoS CORFU 2018 **347**, 152 (2019).

[22] G. Odyniec, EPJ Web Conf. **95**, 03027 (2015).

[23] T. Ablyazimov *et al.* (CBM Collaboration), Eur. Phys. J. A **53**, 60 (2017).

[24] C. Sturm, B. Sharkov, and H. Stoecker, Nucl. Phys. A **834**, 682c (2010).

[25] V. Kekelidze, A. Kovalenko, R. Lednicky, V. Matveev, I. Meshkov, A. Sorin, and G. Trubnikov, Nucl. Phys. A **956**, 846 (2016).

[26] H. Sako *et al.* (J-PARC Heavy-Ion Collaboration), Nucl. Phys. A **931**, 1158 (2014); **956**, 850 (2016).

[27] H. Petersen, J. Steinheimer, G. Burau, M. Bleicher, and H. Stocker, Phys. Rev. C **78**, 044901 (2008).

[28] P. Batyuk, D. Blaschke, M. Bleicher, Y. B. Ivanov, Iu. Karpenko, S. Merts, M. Nahrgang, H. Petersen, and O. Rogachevsky, Phys. Rev. C **94**, 044917 (2016).

[29] C. Shen and B. Schenke, Phys. Rev. C **97**, 024907 (2018).

[30] G. S. Denicol, C. Gale, S. Jeon, A. Monnai, B. Schenke, and C. Shen, Phys. Rev. C **98**, 034916 (2018).

[31] Y. Akamatsu, M. Asakawa, T. Hirano, M. Kitazawa, K. Morita, K. Murase, Y. Nara, C. Nonaka, and A. Ohnishi, Phys. Rev. C **98**, 024909 (2018).

[32] C. Alt *et al.* (NA49 Collaboration), Phys. Rev. C **68**, 034903 (2003).

[33] L. Adamczyk *et al.* (STAR Collaboration), Phys. Rev. Lett. **112**, 162301 (2014).

[34] L. Adamczyk *et al.* (STAR Collaboration), Phys. Rev. Lett. **120**, 062301 (2018).

[35] R. J. M. Snellings, H. Sorge, S. A. Voloshin, F. Q. Wang, and N. Xu, Phys. Rev. Lett. **84**, 2803 (2000).

[36] H. Petersen, Q. Li, X. Zhu, and M. Bleicher, Phys. Rev. C **74**, 064908 (2006).

[37] V. P. Konchakovski, W. Cassing, Y. B. Ivanov, and V. D. Toneev, Phys. Rev. C **90**, 014903 (2014).

[38] D. H. Rischke, Y. Pursun, J. A. Maruhn, H. Stoecker, and W. Greiner, Acta Phys. Hung. A **1**, 309 (1995).

[39] J. Brachmann, S. Soff, A. Dumitru, H. Stöcker, J. A. Maruhn, W. Greiner, L. V. Bravina, and D. H. Rischke, Phys. Rev. C **61**, 024909 (2000).

[40] Y. B. Ivanov and A. A. Soldatov, Phys. Rev. C **91**, 024915 (2015); Eur. Phys. J. A **52**, 10 (2016).

[41] B. A. Li and C. M. Ko, Phys. Rev. C **58**, R1382 (1998).

[42] Y. Nara, H. Niemi, A. Ohnishi, and H. Stöcker, Phys. Rev. C **94**, 034906 (2016).

[43] Y. Nara, H. Niemi, J. Steinheimer, and H. Stoecker, Phys. Lett. B **769**, 543 (2017).

[44] J. Steinheimer, J. Auvinen, H. Petersen, M. Bleicher, and H. Stöcker, Phys. Rev. C **89**, 054913 (2014).

[45] J. Xu *et al.*, Phys. Rev. C **93**, 044609 (2016); Y. X. Zhang *et al.*, *ibid.* **97**, 034625 (2018); A. Ono *et al.*, *ibid.* **100**, 044617 (2019).

[46] G. F. Bertsch, H. Kruse, and S. Das Gupta, Phys. Rev. C **29**, 673(E) (1984); **33**, 1107 (1986); G. F. Bertsch and S. Das Gupta, Phys. Rep. **160**, 189 (1988).

[47] W. Cassing, V. Metag, U. Mosel, and K. Niita, Phys. Rep. **188**, 363 (1990).

[48] H. Kruse, B. V. Jacak, J. J. Molitoris, G. D. Westfall, and H. Stöcker, Phys. Rev. C **31**, 1770 (1985); H. Kruse, B. V. Jacak, and H. Stöcker, Phys. Rev. Lett. **54**, 289 (1985);

[49] J. Aichelin and H. Stoecker, Phys. Lett. B **176**, 14 (1986); J. Aichelin, Phys. Rep. **202**, 233 (1991).

[50] G. M. Welke, M. Prakash, T. T. S. Kuo, S. Das Gupta, and C. Gale, Phys. Rev. C **38**, 2101 (1988); C. Gale, G. M. Welke, M. Prakash, S. J. Lee, and S. Das Gupta, *ibid.* **41**, 1545 (1990).

[51] B. A. Li, L. W. Chen, and C. M. Ko, Phys. Rep. **464**, 113 (2008).

[52] O. Buss *et al.*, Phys. Rep. **512**, 1 (2012).

[53] C. Pinkenburg *et al.* (E895 Collaboration), Phys. Rev. Lett. **83**, 1295 (1999).

[54] P. Danielewicz, R. A. Lacey, P. B. Gossiaux, C. Pinkenburg, P. Chung, J. M. Alexander, and R. L. McGrath, Phys. Rev. Lett. **81**, 2438 (1998).

[55] G. Rai *et al.* (E895 Collaboration), Nucl. Phys. A **661**, 162 (1999).

[56] P. Hillmann, J. Steinheimer, and M. Bleicher, J. Phys. G **45**, 085101 (2018).

[57] Y. Nara and A. Ohnishi, Nucl. Phys. A **956**, 284 (2016).

[58] B. Blattel, V. Koch, W. Cassing, and U. Mosel, Phys. Rev. C **38**, 1767 (1988); B. Blaettel, V. Koch, and U. Mosel, Rept. Prog. Phys. **56**, 1 (1993).

[59] C. M. Ko, Q. Li, and R. C. Wang, Phys. Rev. Lett. **59**, 1084 (1987); C. M. Ko and Q. Li, Phys. Rev. C **37**, 2270 (1988); Q. Li, J. Q. Wu, and C. M. Ko, *ibid.* **39**, 849 (1989); H. T. Elze, M. Gyulassy, D. Vasak, H. Heinz, H. Stoecker, and W. Greiner, Mod. Phys. Lett. A **2**, 451 (1987).

[60] C. Fuchs and H. H. Wolter, Nucl. Phys. A **589**, 732 (1995).

[61] P. K. Sahu, A. Hombach, W. Cassing, and U. Mosel, Nucl. Phys. A **640**, 493 (1998); P. K. Sahu, W. Cassing, U. Mosel, and A. Ohnishi, *ibid.* **672**, 376 (2000); P. K. Sahu and W. Cassing, *ibid.* **712**, 357 (2002).

[62] C. Fuchs, E. Lehmann, L. Sehn, F. Scholz, T. Kubo, J. Zipprich, and A. Faessler, Nucl. Phys. A **603**, 471 (1996).

[63] Y. Nara, N. Otuka, A. Ohnishi, K. Niita, and S. Chiba, Phys. Rev. C **61**, 024901 (1999).

[64] H. Sorge, H. Stoecker, and W. Greiner, Ann. Phys. **192**, 266 (1989).

[65] H. Sorge, Phys. Rev. C **52**, 3291 (1995).

[66] S. A. Bass *et al.*, Prog. Part. Nucl. Phys. **41**, 255 (1998).

[67] M. Bleicher *et al.*, J. Phys. G **25**, 1859 (1999).

[68] J. Boguta and A. R. Bodmer, Nucl. Phys. A **292**, 413 (1977).

[69] J. Boguta and H. Stoecker, Phys. Lett. B **120**, 289 (1983).

[70] B. M. Waldhauser, J. A. Maruhn, H. Stöcker, and W. Greiner, Phys. Rev. C **38**, 1003 (1988).

[71] A. Komar, Phys. Rev. D **18**, 1881 (1978); **18**, 1887 (1978); **18**, 3617 (1978).

[72] D. Oliinychenko and H. Petersen, Phys. Rev. C **93**, 034905 (2016).

[73] T. Maruyama, K. Niita, T. Maruyama, S. Chiba, Y. Nakahara, and A. Iwamoto, Prog. Theor. Phys. **96**, 263 (1996); D. Mancusi, K. Niita, T. Maruyama, and L. Sihver, Phys. Rev. C **79**, 014614 (2009).

[74] R. Marty and J. Aichelin, Phys. Rev. C **87**, 034912 (2013).

[75] G. Q. Li, C. M. Ko, and G. E. Brown, Phys. Rev. Lett. **75**, 4007 (1995); Nucl. Phys. A **606**, 568 (1996).

[76] A. B. Larionov, O. Buss, K. Gallmeister, and U. Mosel, Phys. Rev. C **76**, 044909 (2007).

[77] W. Cassing, A. Palmese, P. Moreau, and E. L. Bratkovskaya, Phys. Rev. C **93**, 014902 (2016); A. Palmese, W. Cassing, E. Seifert, T. Steinert, P. Moreau, and E. L. Bratkovskaya, *ibid.* **94**, 044912 (2016).

[78] K. Weber, B. Blattel, V. Koch, A. Lang, W. Cassing, and U. Mosel, Nucl. Phys. A **515**, 747 (1990).

[79] T. Hirano and Y. Nara, Prog. Theor. Exp. Phys. **2012**, 01A203 (2012).

[80] P. Moreau, O. Soloveva, L. Oliva, T. Song, W. Cassing, and E. Bratkovskaya, Phys. Rev. C **100**, 014911 (2019).

[81] H. Liu *et al.* (E895 Collaboration), Phys. Rev. Lett. **84**, 5488 (2000).

[82] H. Appelshauser *et al.* (NA49 Collaboration), Phys. Rev. Lett. **80**, 4136 (1998).

[83] P. Shanmuganathan (STAR Collaboration), Nucl. Phys. A **956**, 260 (2016).

[84] L. Adamczyk *et al.* (STAR Collaboration), Phys. Rev. C **86**, 054908 (2012).

[85] A. Andronic *et al.* (FOPI Collaboration), Phys. Lett. B **612**, 173 (2005).

[86] H. Sorge, Phys. Rev. Lett. **78**, 2309 (1997).

[87] J. Chen, X. Luo, F. Liu, and Y. Nara, Chin. Phys. C **42**, 024001 (2018).

[88] Y. Nara, H. Niemi, A. Ohnishi, J. Steinheimer, X. Luo, and H. Stoecker, Eur. Phys. J. A **54**, 18 (2018).

[89] Y. Nara, J. Steinheimer, and H. Stoecker, Eur. Phys. J. A **54**, 188 (2018).

[90] C. Zhang, J. Chen, X. Luo, F. Liu, and Y. Nara, Phys. Rev. C **97**, 064913 (2018).

[91] M. Isse, A. Ohnishi, N. Otuka, P. K. Sahu, and Y. Nara, Phys. Rev. C **72**, 064908 (2005).

[92] J. Barrette *et al.* (E877 Collaboration), Phys. Rev. C **56**, 3254 (1997).

[93] S. He, X. Luo, Y. Nara, S. Esumi, and N. Xu, Phys. Lett. B **762**, 296 (2016).

[94] J. Steinheimer, Y. Wang, A. Mukherjee, Y. Ye, C. Guo, Q. Li, and H. Stoecker, Phys. Lett. B **785**, 40 (2018).

[95] Y. Ye, Y. Wang, J. Steinheimer, Y. Nara, H. J. Xu, P. Li, D. Lu, Q. Li, and H. Stoecker, Phys. Rev. C **98**, 054620 (2018).

[96] K. Fukushima, Phys. Rev. C **91**, 044910 (2015).